Spring 2022

Mechanical Stabilization by Cyclic Compression of Composite Polymer Electrolytes for Lithium-Ion Batteries

Nishad Mulay
San Jose State University

MECHANICAL STABILIZATION BY CYCLIC COMPRESSION OF COMPOSITE POLYMER ELECTROLYTES FOR LITHIUM-ION BATTERIES

A Thesis

Presented to

The Faculty of the Department of Mechanical Engineering

San José State University

In Partial Fulfillment

of the Requirements for the Degree

Master of Science

by

Nishad Mulay

May 2022

The Designated Thesis Committee Approves the Thesis Titled

MECHANICAL STABILIZATION BY CYCLIC COMPRESSION OF COMPOSITE POLYMER ELECTROLYTES FOR LITHIUM-ION BATTERIES

by

Nishad Mulay

APPROVED FOR THE DEPARTMENT OF MECHANICAL ENGINEERING

SAN JOSÉ STATE UNIVERSITY

May 2022

Sang-Joon Lee, Ph.D.	Department of Mechanical Engineering
Dahyun Oh, Ph.D.	Department of Chemical and Materials Engineering
Min Hwan Lee, Ph.D.	Department of Mechanical Engineering, UC Merced

ABSTRACT

MECHANICAL STABILIZATION BY CYCLIC COMPRESSION OF COMPOSITE POLYMER ELECTROLYTES FOR LITHIUM-ION BATTERIES

by Nishad Mulay

Composite polymer electrolytes (CPEs) for lithium-ion batteries provide an effective balance of ionic conductivity, mechanical robustness, and safety. Loss of charge capacity, however, is caused by multiple contributing factors, such as dendrite formation, changes in polymer crystallization, and reconfiguration of porous electrodes. In this thesis we specifically examine mechanical changes in the composite electrolyte layer. The hypothesis of this investigation is that the addition of rigid particles to a polymer electrolyte counteracts the fatigue softening effect caused by cyclic dimensional changes, as would be experienced during charge and discharge cycles. We apply cyclic compression to mimic stress cycling that is caused by asymmetric volume changes during charging cycles between anode and cathode. Using a representative composite electrolyte consisting of $Li_{6.4}La_3Zr_{1.4}Ta_{0.6}O_{12}$ (LLZTO) particles in polyethylene oxide (PEO) with bis(trifluoromethane) sulfonimide (LiTFSI), we experimentally measure stress-strain response, peak stress during cyclic compression, stress relaxation, and surface topography. When tested for 500 cycles at 30% compressive strain, the average normalized peak stress for specimens containing LLZTO was reduced by 12%, compared to a reduction of 25% without LLZTO. These experiments reveal how rigid particles can favorably alter the mechanical response of a composite electrolyte and contribute to more consistent mechanical behavior over the life of lithium-ion batteries.

ACKNOWLEDGMENTS

This work was sponsored in part by the Mechanics of Materials and Structures program of the National Science Foundation (Award #2125192) and supported by the Charles W. Davidson College of Engineering at San Jose State University. I would like to thank Dr. Sang-Joon (John) Lee for his mentorship and guidance throughout this investigation. I would like to thank Dr. Dahyun Oh and the members of the Chemical and Materials Engineering lab at San José State University for specimen fabrication and experiment collaboration. I would also like to thank Dr. Min Hwan Lee for his insight and guidance. I would like to gratefully acknowledge Medtronic (Milpitas, California site) for donation of the Instron system used for data collection. Lastly, I would like to thank my friends and family for their continued support.

TABLE OF CONTENTS

LIST OF FIGURES

LIST OF SYMBOLS AND ABBREVIATIONS

Symbol	Units	Description
G_0	-	Spring constant of generalized Maxwell model
μ_0	-	Dashpot constant of generalized Maxwell model
μ_i	-	Dashpot constant of the ith element
t	s	Time
τ_i	s	Time constant of the ith term in the exponential fit
z	µm	Vertical position values of optical profilometry scan
R_q	µm	Root mean square of the surface roughness
$\eta(x,y)$	µm	Residual surface values at a given point (x,y)
M	-	Total number of data points in x-direction
N	-	Total number of data points in y-direction
X	-	Number of empty pixels
n	-	Number of replicates
a	kPa	Exponential fit parameter for magnitude
b	-	Exponential fit parameter for linearity
σ	kPa	Stress
ε	-	Strain
p	-	P-value

Abbreviation	Full Spelling
CPE	composite polymer electrolytes
LLZTO	$Li_{6.4}La_3Zr_{1.4}Ta_{0.6}O_{12}$
PEO	polyethylene oxide
LiTFSI	lithium bis(trifluoromethanesulfonyl)imide
LLZO	$Li_{6.4}La_3Zr_{1.4}O_{12}$
CSDICE	Coefficient of Strain Dependent Ion Conductivity Enhancement
PDMS	polydimethylsiloxane
EIS	electrochemical impedance spectroscopy
GMM	generalized Maxwell model
RILT	regularized inverse Laplace transform
ACN	acetonitrile

PTFE	polytetrafluoroethylene
SED	strain energy density

1. INTRODUCTION

1.1 Background

The increasing demand for battery power has led to the development of several material systems for lithium-ion batteries. Composite polymer electrolytes (CPE) are safer than the more common organic liquid electrolytes due to their decreased flammability and resistance to overheating. However, the liquid electrolytes have much better ionic conductivity than the CPE. Rigid materials such as $Li_{6.4}La_3Zr_{1.4}Ta_{0.6}O_{12}$ (LLZTO) or $Li_{6.4}La_3Zr_{1.4}O_{12}$ (LLZO) are some of the more promising filler materials for enhancing ionic conductivity in the CPE [1]. Very little is known about the mechanics of these recent polymer electrolytes and how they respond to the internal stresses caused by volumetric changes in the battery. At lower rates of charge, where temperature does not fluctuate, the internal components of a battery can experience up to 2% strain. However, when factoring in temperature increases and thermal swelling at higher charging rates, the internal strain on the battery can reach up to 15% [2]. As battery technology continues to move toward faster charging speeds, these internal strains will play a larger role in the health and performance of the battery electrolytes.

1.2 Hypothesis

This thesis investigates the relationship between the mechanical loading history of a composite polymer electrolyte containing rigid particles and its long-term mechanical behavior. Mechanical loading can be manifested as a static compress-and-hold process or a cyclic sequence of compression and relaxation to free-state.

Specifically, The hypothesis of this investigation is that the addition of rigid particles to a composite polymer electrolyte counteracts the fatigue softening effect caused by cyclic compression. The reasoning for this mitigation of softening is structural stabilization provided by the presence of the particles.

Two important quantitative metrics are the normalized peak stresses and the viscoelastic time constants of the composite electrolytes. It is envisioned that quantitative results from this work will help to determine how to reduce fatigue softening of electrolytes as they experience volumetric changes and internal stresses throughout the charging and discharging cycle.

1.3 Significance

Prior research has been conducted on different CPEs, combining the thermal resistivity of polymer electrolytes and the ionic conductivity of garnet-type rigid particles [1]. Much of this work looks towards the effect of rigid particles to the ionic conductivity of the polymer, comparing the conductivities of the CPE with and without the rigid particles [3]. Some of this published research also investigates the mechanical properties of the CPE, conducting stress-strain tests and determining the strength of the polymers [4]. This thesis focuses on the effects of rigid particles to the prolonged mechanical response of the CPE. Rather than investigate the ionic conductivity or characterize the instantaneous stress-strain response of the electrolytes, this thesis will look to compare the mechanical response of the CPEs over a longer period of time and under repeated mechanical loads.

Connecting the mechanical response to battery performance, thermal expansion from high charging rates cause electrolytes to experience up to 15% strain when approaching a full state of charge [2]. These expansion measurements were taken on a lithium-ion cell with a nickel/manganese/cobalt-oxide cathode. The charging speeds of batteries are quantified by C-rates. The C-rate is calculated by taking the inverse of the charging time, where a C-rate of 0.4C would equate to 2.5 hours charging time and a C-rate of 5C would equate to 0.2 hours charging time. The study found that at low charge rates of 0.4C, the battery cell only experienced 2% strain while at higher charge rates of 5C, the battery experienced 15% strain. Stress-strain curves show how an electrolyte will respond at higher strains and how much stress the electrolyte might experience in those situations. Each charge cycle for a battery can be up to three hours, depending on the charging rate, with this specific study using an $LiCoO_2$ cathode [5]. The viscoelastic response quantifies how an electrolyte behaves throughout a single charge cycle. A viscous response could be detrimental to battery performance, as the instantaneously softened electrolyte would not be able to maintain a high contact pressure between the anode and cathode. Continued performance and battery health later in a battery's cycle life is another indication of an efficient battery with most lithium-ion batteries having a battery cycle life between 600 and 800 cycles [6]. Therefore, the normalized peak stress results take a large-scale approach to the mechanical response of the electrolytes over the whole life of the battery. Through both the stress relaxation and cyclic compression results, the 500 nm LLZTO electrolytes exhibit a more stable response, with less fatigue softening from both cyclic and constant compression. Fatigue softening in electrolytes can lead to

weaker contact pressure between battery components, resulting in a decrease in battery capacity and longevity [7]. Some of the specific studies discussed further in the related work section use solid electrolytes with alkali metal anodes and polymer electrolyte membranes electrolysis cells. This investigation will produce knowledge about how the polymer electrolytes withstand and respond to internal forces as well as how the internal forces that act upon the electrolytes over the course of the charge-discharge cycles affect the contact pressure of battery components within lithium ion batteries.

2. RELATED WORK

2.1 Volume Change of Electrolytes During the Charging Cycle

There are two prevalent methods for measuring the electrochemical expansion of the CPE. One method is to limit the force applied to the battery and measure the displacement and the other is to limit the displacement of the battery and measure the force that it exerts. Koerver et al. took the latter approach, using a series of springs to create a model for the expansion force of the battery [8]. Koerver was able to model an ideal representation using two springs in a series, where the lengths of the springs were proportional to the fractional volumes of the different phases of the cathode. This combination of springs produced an easier way to calculate the effective Young's modulus of the system. A simpler and more straightforward way to measure the volume change is to apply a constant load to the battery and measure the displacement. Lee et al. placed a battery between two parallel plates before applying a 300 g load [9]. Lee then used a thickness gauge and an automatic data logger to measure the displacement. Barker used a linear voltage displacement transducer with their thickness gauge to get a finer resolution measurement of the dimensional changes than the automatic data logger from Lee's research [10]. Lee used this apparatus to test the volumetric expansion of different batteries during the charge discharge cycle. They found that depending on the battery, the volume expanded by 2% to 4% at a slow charging speed of 0.05C.

2.2 Mechanical Testing of Polymer Electrolytes

Another approach for studying polymer electrolytes is through stress-strain testing. Kelly et al. investigated the ionic conductivity of polyethylene oxide (PEO) electrolytes and how

the conductivity fluctuates under tensile strain [3]. Their main focus was the functionality of battery electrolytes when stretched. This experiment used impedance spectroscopy, which sends an excitation signal through the material to measure the resistance and capacitance. The main takeaways from this research are that the more the electrolyte is stretched, the lower the impedance, leading to an increase in conductivity. Kelly found that the Coefficient of Strain Dependent Ion Conductivity Enhancement (CSDICE) remained similar regardless of the plane of measurement of the CPE. The consistency suggests that CSDICE is an isotropic property and relates more with how the polymer chains react to each other rather than which direction they are stretched.

Lee et al. ran compressive tests on polydimethylsiloxane (PDMS) elastomers [4]. They added a curing agent to the PDMS and observed how the mechanical properties changed as the concentration of the curing agent increased. This group ran two different tests, a compression test to failure and another cyclic compression test in which they alternated between 0% strain and 20% strain for 100 cycles. The viscoelastic response they observed exhibited some hysteresis, which represented dissipated energy while the sample was under compression. However, the amount of hysteresis decreased as the compressive cycling on the battery increased. Another effect of the cyclic compression was strain hardening which they attributed to increases in both peak stress and elastic modulus as the battery was cycled.

Sauerteig et al. took the approach of using electrochemical impedance spectroscopy to measure the stress-strain behavior of their 10 A·h capacity hybrid electric vehicle cell [11]. They ran the spectroscopy by creating 10 mV perturbations and cycling the frequency from

100 kHz to 1 Hz at a rate of 10 frequency points per decade. Their results showed that the stress-strain curve was nonlinear, which was consistent with other porous polymers. However, Sauerteig observed some stiffening in the electrolyte, found by taking the derivative of the compression curve. This stiffening was attributed to electrolyte decomposition products that were created from the compressive cycling. Borgardt et. al. used stress relaxation to study the effects of clamping pressure on the cell performance of polymer electrolyte membranes [7]. They concluded that stress relaxation in polymer electrolyte membranes lead to a loss of pressure and a decline in cell performance.

Patra et al. developed a lithium-ion polymer electrolyte membrane using polyethylene oxide (PEO) and $LiClO_4$ and studied its microstructure variations while applying external stress [12]. The microstructural evolution showed dislocations in the crystallites of PEO at larger strains, leading to the formation of amorphous regions which soften the matrix. Patra applied cyclic strains of 2% in both compression and tension. They discovered that compressive strain caused fatigue softening, decreasing the stress from 2.7 kPa to 2.5 kPa over 200 minutes of mechanical cycling. Conversely, tensile strain caused fatigue hardening, increasing the stress from 0.2 MPa to 0.3 MPa over 200 minutes of mechanical cycling.

Mansouri et al. took a microscopic approach to investigate the cause behind the degradation and pseudoelasticity of mechanical properties in composite materials, seen through cyclic tensile testing [13]. They used monotonic loading and cyclic tensile tests to evaluate inelastic phenomena similar to what are seen in this thesis, such as residual strain and hysteresis. Mansouri et al. used a PDMS matrix and glass-fiber reinforcement and were

able to look at micrographs of the composites through digital image correlation. The micrographs helped them attribute the permanent deformations in the composite to interfacial debonding between the matrix and the fiber as opposed to the individual matrix or fiber materials weakening separately.

2.3 Effects of Thermal Expansion on Battery Cells

Looking at the thermal expansion of batteries, Oh et al. was able to capture information by running two similar experiments. In the first experiment, they measured the thermal swelling of the cell from 5 ℃ to 45 ℃ to attain the total thermal expansion with the surrounding fixture and sensor of their system included [14]. In the second experiment, Oh replaced the cell with an aluminum block of the same dimensions. Since the coefficient of thermal expansion for the aluminum was known, they were able to separate the two thermal expansion values and find the excess expansion of the fixture and sensor. They were then able to use those values to isolate the expansion of the cell from the first experiment. In a separate study, Oh et al. ran a test to determine the thermal expansion of an electric vehicle battery cell [2]. This time, Oh charged the cell in an insulated environment where the cell expansion could be attributed to both thermal and electrochemical expansion. Subsequently, they ran the same experiment in a thermal chamber that could regulate the temperature and counteract the thermal expansion. By comparing the results from both experiments, they were able to find a 1.5% difference in expansion at low discharge rates of 0.4C. The volumetric differences increased as the battery approached higher discharge rates. Furthermore, the expansion was not uniform, with the center of the cell expanding more than

the edges. At higher discharge rates, reaching up to 5C, thermal swelling played a much larger role, increasing the strain on the battery by a factor of six. The internal strain reaches its peak after the battery is completely charged and at the beginning of the discharge process, when the temperature of the battery is the highest. Heinz et al. studied Na-$NiCl_2$ cells under high temperatures. These cells performed well because the sodium melted at higher temperatures, surrounding the $NiCl_2$ in a molten electrolyte base that did not have a major effect on the charging functionality [15]. However, the concern for Heinz was that the pressure changes resulting from the high-temperature molten sodium created stresses that were detrimental to the cell. By testing the pressure changes in multiple cell designs, Heinz found that hollow tubular cells fared better against the increased stress than conventional planar cells.

2.4 Optical Imaging of Particles in Battery Electrolytes

Optical imaging can be utilized to observe the particles within the battery cell. Jones et al. used digital image correlation to measure the strains and cracks that arose in Li-ion batteries as they were charged [16]. Jones took multiple images of the electrode surface via an in situ image capture device. They then used the digital image correlation software to measure changes in strain throughout the cycle. Jones found that the cell expanded by 1.41% during lithiation and contracted by 1.33% during delithiation. Xie et al. created an optical acquisition system using a telecentric lens to monitor the deformation of their silicon electrode in real time [17]. With the use of their system, Xie was able to find that the compressive stress of the composite increased as lithium particles were added to the silicon

electrode. They also discovered that softening the silicon electrode could alleviate stress from lithium particles. Rees et al. used magnetic resonance imaging to observe the growth of sodium dendrites in solid-state batteries [18]. Using this imaging technology, dendrites with a skin depth of 11 μm were found. These dendrites lead to cell failure because of how they penetrate the cell and cause short circuits. Therefore the magnetic resonance imaging was extremely useful in observing the dendrite growth so that new solutions could be engineered to prevent such failures. Blanquer et al. used optical fiber Bragg grating sensors embedded in battery electrolytes to monitor chemo-mechanical stresses locally at the interfaces between the electrodes and the electrolytes [19]. They measured the changes in stress at three different locations; the cathode-electrolyte interface, the anode-electrolyte interface, and the anode. At all three locations the change in stress reached a maximum near the end of the electrical charging cycle of the battery.

Sedimentation is the process where particles in a polymer settle closer together and aggregate based on the particle size. The rate of sedimentation depends on the density differences between the particles and the polymer. Filler-matrix interaction is controlled by the interfacial interaction between filler and matrix. It is connected with particle-particle interaction as a function of the particle concentration. In this study, Samal placed varying sizes of iron particles in a silicone elastomer [20]. They found that the larger particles tend to group together and sink to the bottom of the polymer. Conversely, they also found that if the particle sizes are uniform then the particles don’t group up at the bottom. Rather, there are

still some filler-matrix interactions that have a tendency to cause grouping and structural stabilization.

2.5 Effects of Mechanical Compression on Electrical Conductivity

Looking closer at the effects that mechanical compression has on electrical conductivity, Bouziane et al. conducted a study on the electrical contact resistance between different layers of fuel cells. They measured the contact resistance of various gas diffusion layers under cyclic compression using the Transmission Line Method, a method used to find the electrical contact resistance between a metal and a semiconductor [21]. For all seven of the tested gas diffusion layers, Bouziane found a nonlinear decrease in the specific electrical contact resistance as the applied pressure increased. They hypothesized that the stress improved the contact between the gas diffusion layers by increasing the contact surface and decreasing the porosity. The improved contact led to the decrease in measured resistance and the improvement in conductivity. Mason et al. conducted a similar experiment measuring the effects of compression on electrical conductivity in fuel cells [22]. They used electrochemical impedance spectroscopy to differentiate between the contact resistance and the mass transport resistance of the fuel cell. Mason found similar results to Bouziane in which the electrical contact resistance decreased as the fuel cell was compressed. However, the mass transport resistance exhibited an opposing effect, in which the resistance increased as the fuel cells were compressed. The higher mass transport resistance can be attributed to permanent tearing and cracking in the fuel cell due to the applied stress. These competing resistivities

led Mason et al. to conclude that there was an optimal compression limit where both the contact resistance and the mass transport resistance were minimized.

Velez et al. studied the electrochemical response of a lithium-ion battery using a silica-PEO-LiTFSI hybrid solid electrolyte that is similar to the PEO-LiTFSI electrolyte used in this thesis [23]. They used Fourier-transform infrared spectroscopy and electrochemical impedance spectroscopy to observe the ionic conductivity of the solid hybrid electrolyte and its dependency on temperature. Some further relevant precedents set by Velez et al. was their decision to electrochemically cycle their electrolyte 500 times to determine the stability. The amount of cycles was harmonious with the 500 compression cycles that we subjected our electrolytes to, which allowed us to study the mechanical stability of the electrolytes. Furthermore, Velez et al. found that the ionic conductivity of the hybrid solid electrolytes increased with the Li:EO ratio of the LiTFSI and PEO. The relationship between conductivity and material composition confirmed our decision to use a high Li:EO ratio of 43:1 in our composite polymer electrolytes.

2.6 Composite Polymer Electrolyte Material Design

The energy-consuming synthetic method with a long, high-temperature solid state reaction process needed to make $Li_7La_3Zr_2O_{12}$ (LLZO) solid electrolytes is one of the reasons that they are not favored in large-scale applications. Li et al. developed a faster preparation method that adds ceramic-like particles such as Aluminum or Tantalum to the LLZO electrolytes [24]. They found that the low porosity and high phase purities of the garnet ceramic electrolytes allows for a quicker preparation time involving short-period thermal

reactions and leads to a higher ionic conductivity. Li's findings helped to corroborate the decisions made in this thesis to use Tantalum-doped LLZO, also known as LLZTO.

Yin et al. used electrostatic attraction to create a structural framework of PEO and aramid nanofibers with LLZO particles acting as lithium-conducting fillers [25]. They found that the discharge capacity retention of the lithium cell with the PEO/LLZO composite electrolyte after 400 cycles was 88%. The capacity retention supported their hypothesis that the composite electrolyte benefited from improved interfacial compatibility and ionic conductivity. Gupta et al. suspected that the LLZTO particles disrupted the crystallinity in the PEO and studied the ionic transport mechanisms that govern the conductivity in the composite polymer electrolyte [26]. They used a trilaminar cell configuration and electrochemical impedance spectroscopy (EIS) to characterize the ionic transport phenomena. They found that surface impurities of LLZTO particles can cause high interfacial resistances between the electrolyte. However, these high resistances can be mitigated by conducting heat treatments to smoothen the surface of the LLZTO particles and by increasing the lithium salt concentration in the PEO. By combining these two methods, Gupta et al. hypothesized that the composite polymer electrolytes can reach a total cell impedance comparable to the impedances of standard electrolytes in lithium-ion batteries.

2.7 Prior Work

Work prior to this thesis was conducted at San Jose State University with a similar LLZTO and PEO-LiTFSI composite. Halabi developed a compression-testing apparatus to characterize the mechanical properties of composite polymer electrolytes in lithium-ion

batteries [27]. The apparatus was able to mimic the volumetric changes of the battery electrodes as compressive forces were applied to the composite electrolyte. Halabi used a PEO gel specimen at a molecular weight of 10,000 g/mol and explored the effects of adding both TiO_2 and LLZTO particles to the electrolyte. It was found that the addition of LLZTO increased the viscoelastic time constant when compared to the plain-PEO electrolytes. Conversely, the addition of TiO_2 particles decreased the time constant when compared to the plain-PEO electrolytes. These findings corroborated the hypothesis that the type of particles change the reaction with the polymer matrix and can either stiffen or soften the composite. Halabi also tried imaging the particle distributions however was unable to find any substantial rearrangement to rigid particles caused by the compression.

Furthermore, we have also conducted similar compression tests while examining a composite polymer electrolyte with a more conventional ethylene-oxide to lithium ratio for batteries [28]. The findings from these experiments showed that the polymer electrolyte stiffness increased depending on the size of the added rigid particles, with larger particles increasing the stiffness more than smaller particles. Furthermore, I also found that the larger rigid particles decreased the specimen to specimen variability in viscoelastic stress relaxation tests. Furthermore, Abraham investigated the benefit of ionic percolation networks into porous electrodes to alleviate high interfacial resistances between electrolytes and electrodes. An ideal threshold of 14% to 19% was found for the creation of an ionic percolation network. If an excess of ion conductors are added to the polymer, it could lead to a loss of active material weight percent, a loss of conductivity, and an increase in resistive components [29].

3. THEORY

The specific engineering theory in this thesis is the characterization of the viscoelasticity of composite materials and the utilization of lumped-parameter representations such as the generalized Maxwell model (GMM). Ideal elastic materials exhibit a linear stress response with little to no relaxation when compressed and ideal viscous materials exhibit instantaneous relaxation when compressed. Viscoelastic materials exhibit an intermediate response, relaxing over a period of time, rather than instantaneously or not at all [30]. Relaxation time constants are a convenient indication of the viscoelastic characteristics of a material.

The generalized Maxwell model is one method used to model the viscoelastic behavior of materials. It consists of multiple Maxwell cells acting in parallel and scales well with added Maxwell cells correlating to more complicated polymers [31]. Taking a closer look at the Maxwell cells, each cell consists of a spring and a dashpot in series. When a stress is applied to the Maxwell cell, the spring immediately compresses, modeling any instantaneous aspects of the viscoelastic material. The piston of the dashpot slowly compresses after reacting to the instantaneous compression of the spring, modeling any slower aspects of the viscoelastic material [32]. Since different elements in a CPE can have different relaxation times, the amount of Maxwell cells used equates to the number of time constants extrapolated from the GMM [33]. Equation 1 shows the base form of the GMM in which the total stress of a polymer is a sum of the stresses of each element in the polymer.

$$G_0\mu_0 + \sum_{i=1}^{N} G_0\mu_i e^{-t/\tau_i} \quad (1)$$

In equation 1, G_0 represents the spring constant of the Maxwell cells in the GMM, μ_0 represents the dashpot constant in the GMM, μ_i represents the dashpot constant of the ith Maxwell cell, t represents time, and τ_i represents the time constant of the ith Maxwell cell. Regularized inverse Laplace transform (RILT) uses the generalized Maxwell model to determine the time constants and amplitudes of exponential decays from experimental data [34]. The RILT process takes the inverse Laplace transform of a stress relaxation curve using a regularized least squares method to determine an exponential decay fit for the data. Least squares regression analysis minimizes the squares of the distances from the model fit to each data point of the stress relaxation curve.

Regularization is an iterative process used to limit the size of coefficients in least squares methods by adding a penalty term to the error. The main benefit of using regularization over standard least squares methods is that regularization allows for a system to have more variables than observations while still providing a uniquely determined solution [35]. Directly using the generalized Maxwell model would require the user to define the amount of time constants when determining the fit, whether it be one time constant for a monoexponential fit or two time constants for a biexponential fit. The extra flexibility provided by RILT means that we are able to find the best fit without constricting time constants. The RILT method outputs plots of relaxation time distributions shown in Figure 1.

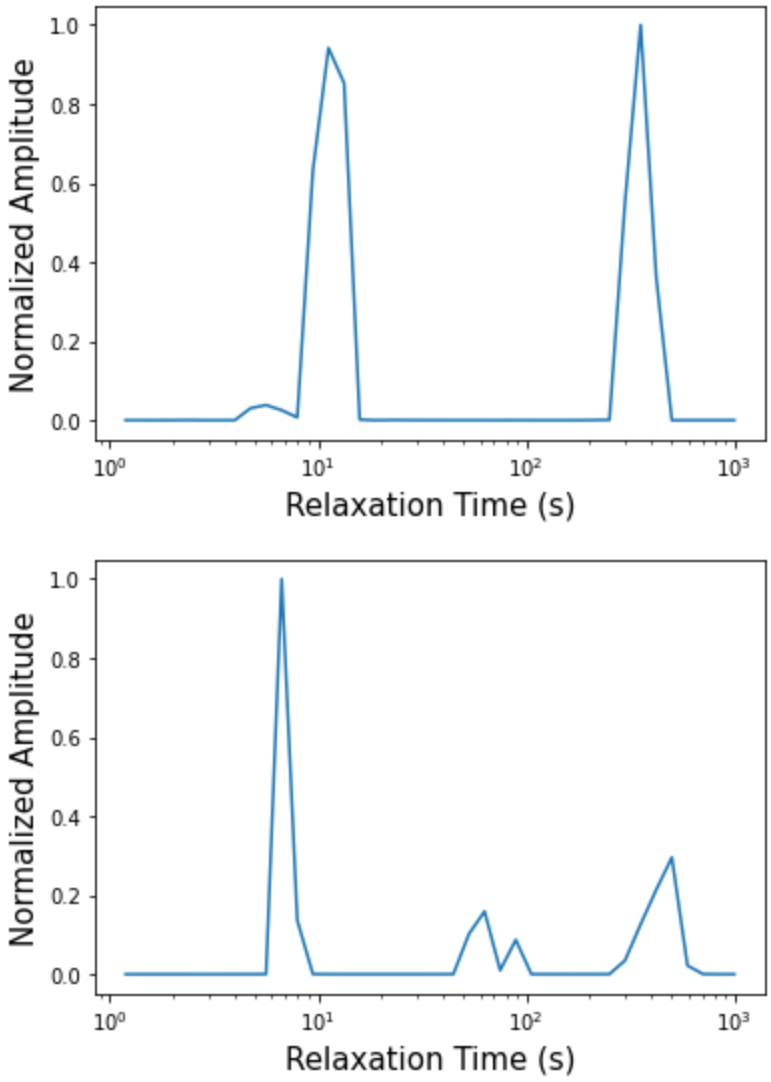

Figure 1. Relaxation time distribution plots from two different stress relaxation curves, one showing a biexponential fit and the other showing a triexponential fit.

As more iterations of RILT are completed and the error between the fit and the data is minimized, the peaks of the relaxation time become more defined. Figure 1 shows outputs from two different stress relaxation curves, showing how one curve may have two distinct time constants and another curve may have three distinct time constants. The distinction

between time constants would be difficult to spot if the fit was limited to a monoexponential or biexponential fit. In order to characterize stress relaxation curves without limiting the time constants of the exponential decay fit, regularized inverse Laplace transform is a fitting model for the viscoelastic behavior of the composite polymer electrolytes.

4. METHODOLOGY

This methodology section will serve to detail the experimental aspects of the investigation into the effects of rigid particles on the mechanical response of a PEO/LLZTO composite polymer electrolyte. The three main facets of this experiment are cyclic compression, stress relaxation, and optical profilometry. The cyclic compression section will detail the process of compressing the specimens as well as the analytical process used to extract relevant data such as strain energy density or normalized peak stress. The stress relaxation section will detail the relaxation procedure and the regularized inverse Laplace transform method used to calculate the time constants. The specimen surface topography section will explain the process of obtaining optical profilometry images and using them to calculate the surface roughness of the specimens. These will supplement the mechanical preconditioning data and be used to further characterize the effects of cycling on the specimens.

4.1 Specimen Fabrication

As a model system for mechanical testing, we used PEO-LiTFSI/LLZTO, which is one of the most promising formulations among CPEs [36]. Composite electrolytes for mechanical testing were fabricated by solution casting using 500 nm LLZTO powder (Ampcera, Inc., Milpitas, California, USA), polyethylene oxide (PEO, M_v = 600,000 g/mol, Sigma-Aldrich Corp., St. Louis, Missouri, USA), and LiTFSI (Gotion, Inc., Fremont, California, USA). Figure 2 shows six fully-fabricated CPE specimens with different sizes of LLZTO particles.

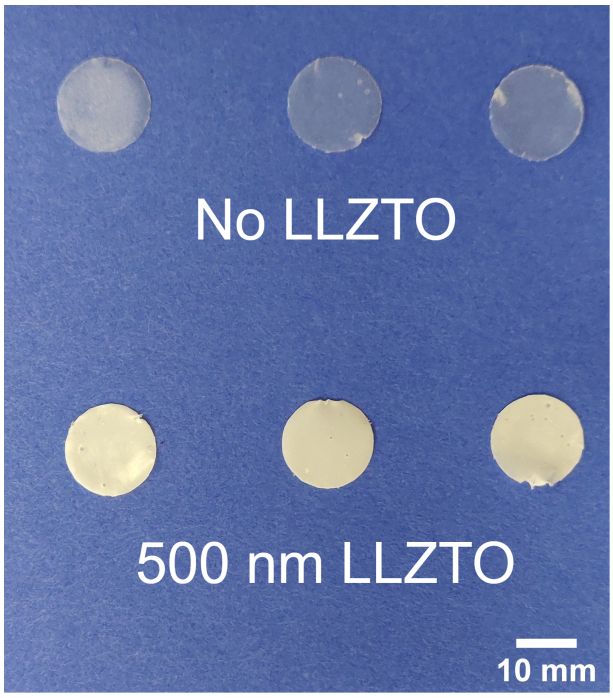

Figure 2. Overview of Polyethylene Oxide (PEO) - Bis(Trifluoromethane) Sulfonimide (LiTFSI) with two different sizes of $Li_{6.4}La_3Zr_{1.4}Ta_{0.6}O_{12}$ (LLZTO) particles.

Particle-loaded films, nominally 50 µm thick, were made by first dissolving the LiTFSI and the corresponding type of LLZTO at 24 wt. % in anhydrous acetonitrile (ACN) and stirring for 30 minutes. PEO was then added to the solution to achieve a 43:1 molar ratio EO:Li, with the mixture stirred at room temperature for 24 hours. Solutions were cast on a flat polytetrafluoroethylene (PTFE) surface and then placed in a vacuum oven at 60 °C for 24 hours to evaporate the solvent. The dried electrolyte films were punched into 15 mm diameter disks for mechanical testing.

4.2 Experimental Workflow

In order to ensure the efficiency of the data collection, the experiment design will be listed in this section. Directly after the specimens are fabricated, they are placed in a nitrogen

chamber for purging and storage. Once the CPE specimens are ready for cycling, they are all taken out of a nitrogen chamber and exposed to the atmosphere at the same time. Figure 3 shows an electrolyte specimen between glass slides and the compression heads of the dynamic testing system. This image is representative of testing conditions throughout the mechanical conditioning procedures.

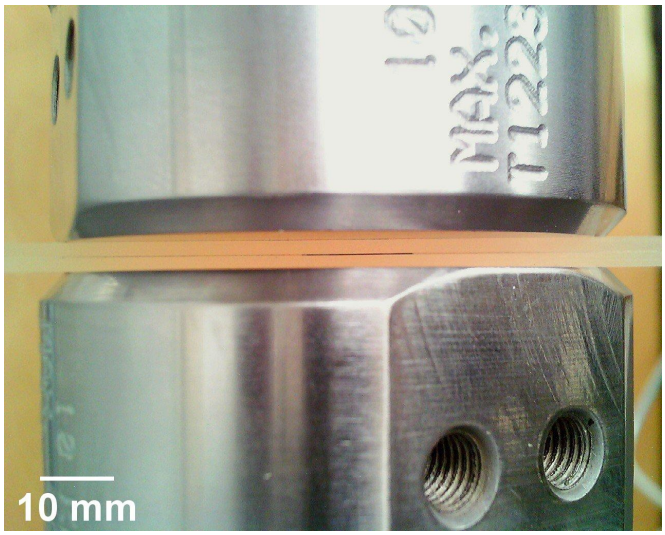

Figure 3. Image showing the electrolyte specimens between glass slides and compression heads of the dynamic testing system.

Figure 4 shows a visual representation of the consecutive mechanical cycling procedures that are conducted on the electrolytes. Also shown are time points for initial and final measurements of specimen thickness and specimen fabrication. The complete mechanical loading of each specimen begins with an initial stress-strain test of 5 compression cycles to 30% strain. The initial test stress-strain test is used to calculate the strain energy density of the specimen as-fabricated.

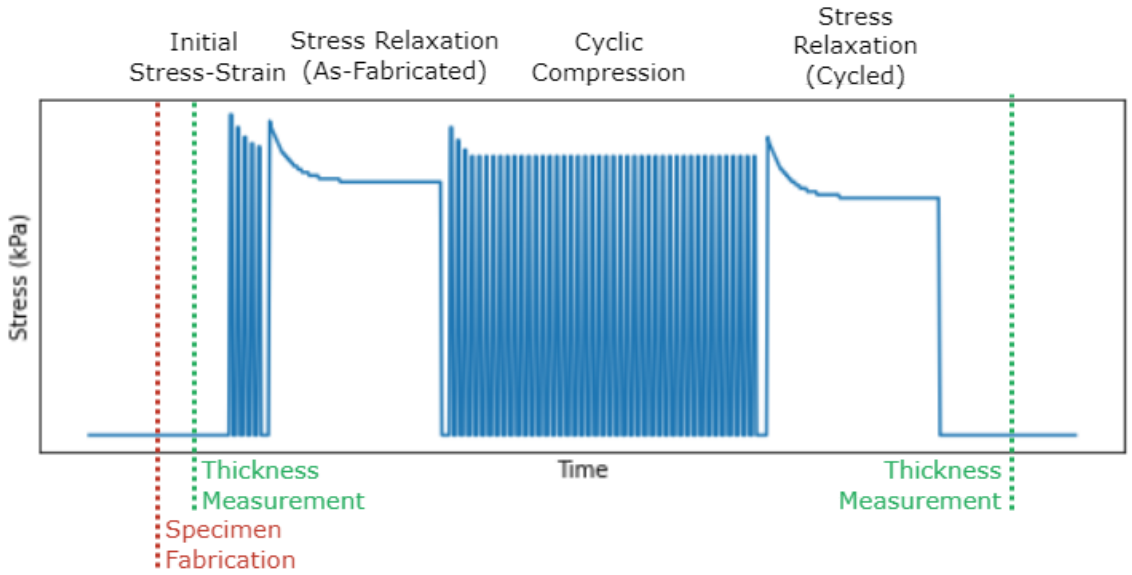

Figure 4. Test protocol for composite polymer electrolytes, showing prescribed loading stages for characterizing nonlinear elasticity, viscoelasticity, and fatigue behavior.

To ensure the "as-fabricated" condition of the specimens, it is important that the strain energy density measurements are taken the first time the specimen is mechanically loaded. Next, a stress relaxation test is performed where the specimens are compressed to 30% strain and the compression is held for ten minutes. After the stress relaxation test, the main cyclic compression test is conducted where the specimen is compressed five hundred times to 30% strain as explained in methodology Section 4.2. Finally, another identical stress relaxation test is conducted after the cyclic compression. The paired stress relaxation tests are helpful for being able to compare the viscoelastic time constants from before and after the cyclic compression and discern differences between the two.

4.3 Cyclic Compression Procedure

All mechanical tests were conducted using an Instron ElectroPuls E1000 dynamic testing system (Instron, Norwood, Massachusetts, USA) outfitted with a 2 kN load cell. The cyclic compression procedure consists of cycling the specimen through five hundred cycles of compression. Our test method is similar to an approach that has been used for cyclic compression of polydimethylsiloxane (PDMS) tested at 20% strain [4]. Since each of the specimens are extremely thin (nominally 50 μm thick), it is difficult to confirm the point at which the upper compression head is in physical contact with the specimen. Accordingly, a preload is set at 70 mN, which ensures that the compression head is in contact with the specimen while exerting a small, consistent contact force on the electrolyte before each cycling run begins. This preload was selected to be equivalent to 2% of the common peak stresses (10 kPa) found when compressing the specimens.

At the beginning of the procedure, the upper compression head is lowered to the preload setpoint over the span of 10 seconds. The driving input to cyclic loading follows a trapezoidal waveform, in which the amplitude is equivalent to 30% of the specimen thickness. For each of the five hundred cycles, the upper compression head starts at the preload setpoint before ramping up to the prescribed amplitude in one second. It then holds at that peak position for 0.5 seconds before ramping back down to the preload displacement and holding for 0.5 seconds again.

In order to mechanically characterize each of the cycled specimens, the strain energy density (SED) is computed from an initial compressive cycling test of five cycles. From

preliminary stress-strain tests, it was found that the specimens exhibit a hysteresis effect in which the first compression cycle has a higher peak stress that levels out by the fifth compression cycle. To provide insight into the mechanical properties of the specimens while accounting for the varying values of the first compression cycle, the stress-strain data from the last four compression cycles is extracted from the initial stress-strain test, excluding the data from the first cycle. An exponential curve is then fitted to the stress-strain curve of the average of the four compression cycles. The area under the curve of this exponential fit curve from 0% to 30% strain is used to calculate the SED values which are useful in comparing the mechanical properties and differences between specimens.

Based on the measured stress values from cyclic compression testing, "fatigue softening" can be quantified concisely in terms of damage, similar to the quantification of damage in the cyclic loading of tendons [37]. Fatigue softening is a viscoelastic effect in which the amount of stress needed for a material to reach similar amounts of strain decreases as the material undergoes prolonged compression.

In this study, the normalized peak stress is used to quantify the fatigue softening of the electrolytes over multiple compression cycles. By isolating the peak of the stress-strain curves, the normalized peak stress from each cycle can be used to characterize the stiffness of the CPE throughout five hundred cycles of compression. Figure 5 shows a representation of how the normalized peak stress can change from cycle to cycle.

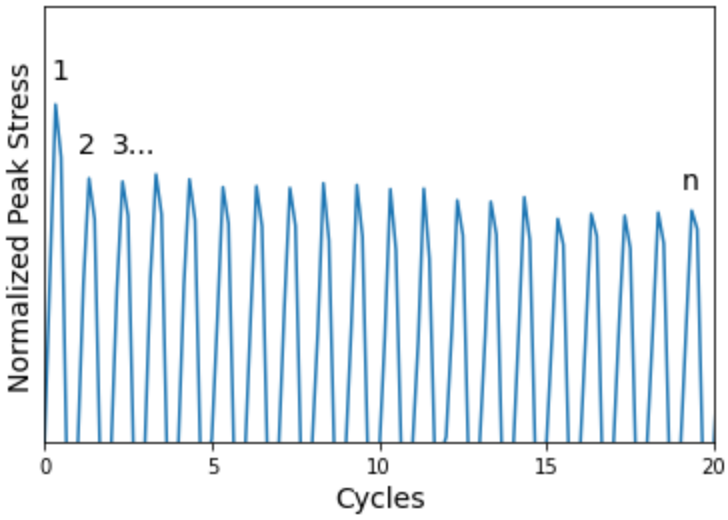

Figure 5. Representation of normalized peak stresses at loading cycles used to quantify fatigue softening. (Representative data from one test are shown for qualitative visualization without numerical scale.)

As well as the individual peak stresses, taking an average of all five hundred peak stresses can provide a good comparison of the mechanical response between different electrolyte specimens

4.4 Stress Relaxation Procedure

In order to determine the viscoelastic response of the composite polymer electrolyte, another method of mechanical preconditioning, stress relaxation, is conducted on the specimens. Stress relaxation tests consist of lowering the upper compression head to the preload setpoint of 70 mN, similar to the process described in the cyclic compression methodology above. The upper compression head is then lowered further to compress the specimen to 30% strain and is held stationary for 10 minutes before lifting. The data from the stress relaxation test are then fit to a curve using the regularized inverse Laplace transform

method and viscoelastic time constants are determined from a least-squares fit to the experimental data, as explained in the theory section.

4.5 Specimen Surface Topography

In order to discern the effect of compressive cycling on the undulations and pores within the composite polymer electrolytes, scanning white light interferometry can be used to scan the topography of the specimens before and after the cyclic compression tests. The purpose of these will be to distinguish any differences on a magnified level and identify the size and location of surface undulations before and after the cycling process.

The optical profilometer outputs a set of vertical position (z) values for the scanned section of the specimen. Measurements were taken at two locations approximately 0.2 mm on each side of a scribed fiducial mark. The fiducial markings are essential in ensuring that the exact same spot can be scanned and measured both before and after cyclic compression. The methodology consists of first finding the central marking on the optical profilometer, then moving to each of the sampling spots and scanning the topography so that the fiducial marking is just out of the frame. For each scan, the root mean square of the surface roughness, R_q, is calculated using equation 2 [38]. The four surface roughness values are then averaged to find the surface roughness of the specimen.

$$R_q = \sqrt{\frac{1}{MN - X} \sum_{j=1}^{N} \sum_{i=1}^{M} \eta^2(x_i, y_j)} \tag{2}$$

In equation 2, $\eta(x,y)$ represents the residual surface values at any given point x and y, M and N represent the total number of data points in the area of the profilometry scan. X

represents the number of empty pixels in the scan that had no number values associated with them. The empty pixels were removed from the profilometry scan data so that an accurate representation of the scanned surface area could be used in the surface roughness calculations.

4.6 Sources of Uncertainty

The main source of uncertainty comes from the dynamic compression machine's positioning system. The positioning system is reliably accurate cycling at any amplitude larger than 10 μm. Since the mechanical preconditioning is conducted at a strain of 30%, the specimen thickness can be about 40 μm on the smallest end, with a specimen thickness of over 60 μm providing more repeatable results. However, it is difficult to achieve consistent specimen thicknesses with some batches being thinner than 30 μm and others falling in the acceptable range. The positioning system was tested in tandem with a contact sensor with a 0.1 μm resolution (GT2, Keyence Corporation, Itasca, Illinois, USA). By comparing the dynamic compression machine's positioning system to the external sensor, it was found that the machine positioning system had an accuracy of 1 μm or 2% of the typical 50 μm thickness for electrolyte specimens.

The accuracy of the 2 kN load cell of the dynamic compression machine is 0.1 N. This accuracy translates to 7% of the 1.5 N peak stresses that are measured during most compression experiments in the thesis. The accuracy of profilometry measurements was checked against a step height calibration standard of 10.027 μm, and determined to be accurate within 87 nm.

5. RESULTS AND DISCUSSION

5.1 Stress-Strain Response

Volumetric expansion of battery components is closely related to the temperature of the components. Therefore, at slow charging rates with little temperature fluctuation, polymer electrolytes only experience 2% strain but at high charging speeds with high temperatures, electrolytes experience up to 15% strain [2]. These higher temperatures usually occur when the battery is close to a full state of charge or just after it has reached a full state of charge. The stress-strain curve shows how an electrolyte will respond at higher strains and how much stress the electrolyte might experience during the charging of a lithium-ion battery. In order to discern the effects of LLZTO particles to composite polymer electrolytes, the stress-strain responses of two sets of specimens were compared. Cyclic compression for five cycles was conducted on a base of PEO with no LLZTO particles and PEO with 500 nm LLZTO particles. Both sets of specimens had 600,000 g/mol PEO at a 43:1 EO:Li ratio and the specimens with 500 nm LLZTO particles had a 24 wt.% of LLZTO.

Figure 6 plots the stress-strain curves for both types of specimens with error bands showing the standard error of the mean. The strain energy density of both types of electrolytes are relatively similar, at 784 J/m^3 and 778 J/m^3. The SED is misleading in this scenario because the 500 nm LLZTO electrolytes have a 57% higher peak stress, reaching 11 kPa, compared to the no LLZTO peak stress, only reaching 7 kPa.

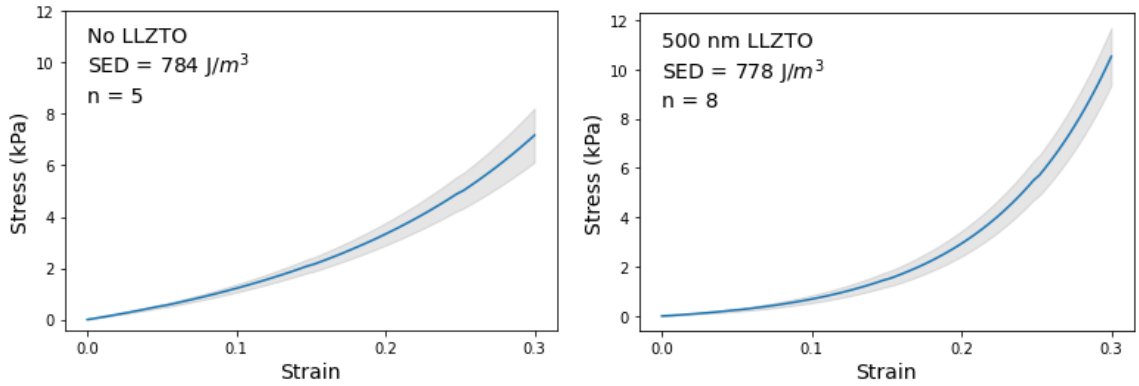

Figure 6. Exponential fit to the stress-strain response of PEO polymer electrolytes and error bands, showing standard error of the mean for (a) PEO without any LLZTO (n = 5 replicates) and (b) PEO with 500 nm LLZTO (n = 8 replicates).

As seen in Figure 6, The low strain response of both CPEs are similar with the stress at 10% strain reaching approximately 1 kPa. However, the high strain response varies greatly, with 500 nm LLZTO specimens experiencing a steep incline in stress to 11 kPa and the no LLZTO specimen remaining much more linear and only reaching 7 kPa. These qualitative observations can be corroborated by the fit parameters of each curve. Equation 3 shows the exponential equation used to model the experimental stress-strain curve with fit parameters a and b.

$$\sigma = a(e^{b\varepsilon} - 1) \tag{3}$$

In equation 3, σ represents the stress exhibited by the specimen, ε represents the strain acting on the specimen, fit parameter a relates to the magnitude of the stress-strain curve, and parameter b relates to the shape and change in slope of the stress strain curve. The fit parameters for the specimens without any LLZTO are a = 1.548 and b = 5.746 and the fit

parameters for specimens with LLZTO are $a = 0.291$ and $b = 12.034$. When compared to the no LLZTO electrolytes, the 500 nm LLZTO electrolytes had a slightly smaller magnitude but a much larger change in slope. The mechanical reasoning behind the differing slopes could be that at low strains, the compression is mainly affecting the PEO, but at higher strains the larger compression begins to affect the LLZTO as well. The mechanical stimulation of the LLZTO particles would explain the change in slope for the 500 nm LLZTO CPEs that is not seen in the no LLZTO CPEs. Adding LLZTO particles to PEO electrolytes increases the stiffness of the composite polymer electrolyte when the battery is being charged at a high rate.

5.2 Normalized Peak Stress

Battery life cycles can fluctuate depending on the different components used in the battery, however, most lithium-ion batteries have a battery life between 600 and 800 cycles [6]. Therefore, the normalized peak stress is used to quantify the stiffness of the CPE as the electrolyte softens over five hundred cycles of compression. Fatigue softening can be detrimental to battery capacity as it reduces the contact pressure between the electrolyte, anode, and cathode [7]. Figure 7 shows the normalized peak stress plotted over five hundred cycles for both no LLZTO and 500 nm LLZTO specimens. All of the specimens in the experiment had 600k g/mol PEO at a 43:1 EO:Li ratio and the specimens with 500 nm LLZTO particles had a 24 wt.% of LLZTO.

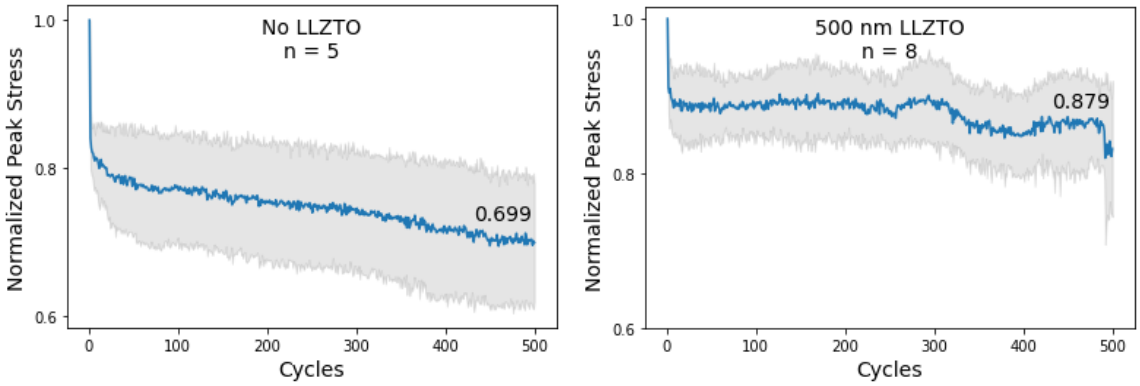

Figure 7. Normalized peak stresses over 500 cycles of PEO polymer electrolytes and error bands showing standard deviation for (a) PEO without any LLZTO (n = 5 replicates)and (b) PEO with 500 nm LLZTO (n = 8 replicates).

As seen in Figure 7, while both types of specimens had an acute initial decrease within the first few cycles, the normalized peak stress for the no LLZTO specimens continued to decrease throughout the five hundred cycles, with an average value of 0.747, softening the electrolyte by 25%. In contrast, the normalized peak stress of the 500 nm LLZTO specimens remained approximately constant after the initial drop and exhibited less fatigue softening when compared to the no LLZTO specimens. The average normalized peak stress of the 500 nm LLZTO specimens over five hundred cycles was 0.879, softening by 12%. Specifically, the addition of LLZTO particles caused a 50% decrease in fatigue softening when compared to the plain PEO specimens (p = 0.012, one-tailed), where p is the probability corresponding to a null hypothesis conclusion [39] Some studies have attributed fatigue softening and changes in mechanical behavior of plain-PEO electrolytes to polymer crystallization [13]. Based on the normalized peak stress results, it could be possible that the LLZTO inhibits this crystallization and diminishes the softening caused by polymer crystallization. To restate the

hypothesis of this investigation, the addition of rigid particles to a composite polymer electrolyte counteracts the fatigue softening effect introduced by cyclic compression. Compared to the 25% fatigue softening of the no LLZTO specimens, the decreased 12% fatigue softening of the 500 nm LLZTO electrolytes provides a more consistent contact pressure within the lithium-ion battery that could improve battery capacity and performance throughout its life.

5.3 Viscoelastic Response

Each individual charge cycle for a lithium-ion battery can take up to three hours [5]. Accordingly, the viscoelastic response describes how an electrolyte behaves throughout a single charge cycle by quantifying the rate at which the specimen relaxes under constant compression. In this study, the time constants are found by fitting an exponential decay fit to the raw stress relaxation data using the regularized inverse Laplace transform method as explained in Section 3. Figure 8 shows an example of the fit created by RILT to the normalized data from the stress relaxation curves. Relaxation time constants from the RILT exponential decay fits seen in Figure 8 were analyzed to quantify the viscoelastic response of these stress relaxation curves. Both the specimens with and without LLZTO used 600k g/mol PEO at a 43:1 EO:Li molar ratio and the specimens with 500 nm LLZTO particles had a 24 wt.% of LLZTO.

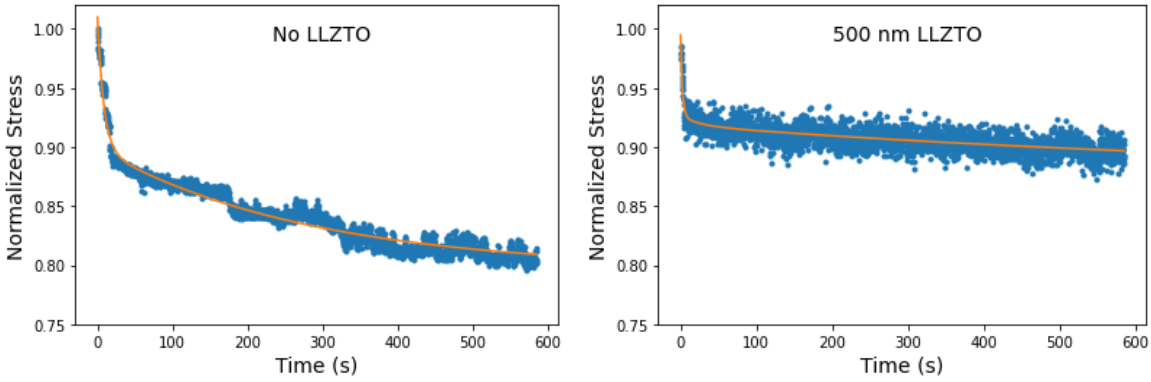

Figure 8. Single-specimen examples of stress relaxation curves with regularized inverse Laplace transform fits for (a) PEO without any LLZTO and (b) PEO with 500 nm LLZTO.

Figure 9 shows the first and second time constants for electrolytes with and without LLZTO and how they change after the cyclic compression process.

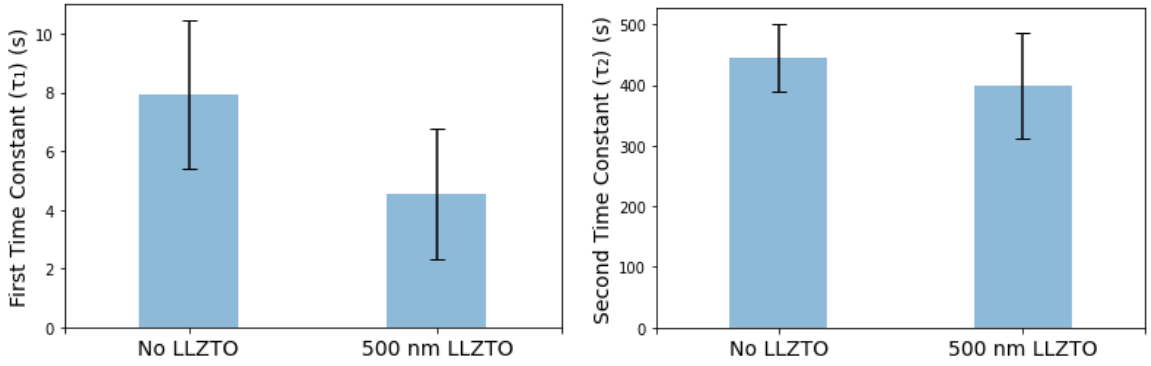

Figure 9. Comparisons of time constants from before and after mechanical cycling for PEO with no LLZTO and with 500 nm LLZTO with figures showing (a) the first time constant and (b) the second time constant. Error bars represent standard error of the mean for $n = 5$ replicates.

Examining the data in Figure 9, the first time constants were 43% faster for 500 nm LLZTO, 4.6 seconds compared to 7.9 seconds for no LLZTO electrolytes. Since batteries charge over longer periods of time the instantaneous response of the electrolytes in the first few seconds were not as informative. Therefore, the more illuminating data came from the

slower second time constants. The second time constants show that the 500 nm LLZTO electrolytes exhibit a similar elastic response with an 11% faster time constant of 398 seconds compared to the no LLZTO time constant of 445 seconds. As seen in Figure 9, the standard deviation was larger for the 500 nm LLZTO for both time constants. The mechanical reasoning behind the larger variability in time constants is that the stress relaxation curves of the 500 nm LLZTO electrolytes were elastic, with almost no relaxation after an initial decline. In order to visualize the time constants from Figure 9, Figure 10 shows an average of the stress relaxation curves for both no LLZTO and 500 nm LLZTO electrolytes.

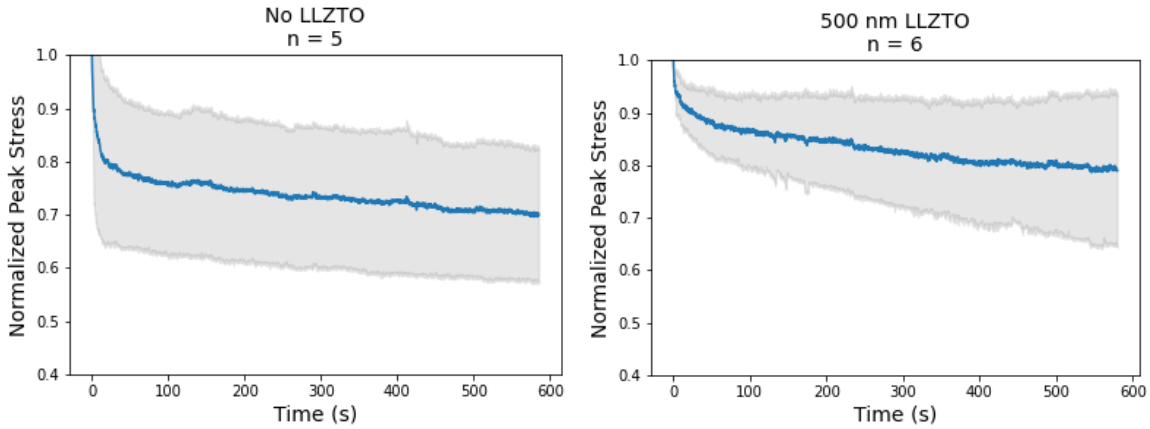

Figure 10. Examples of normalized stress relaxation curves with shaded error bands showing the standard deviation for (a) PEO without any LLZTO (n = 5 replicates) and (b) PEO with 500 nm LLZTO (n = 6 replicates).

Coincidentally, these stress relaxation curves exhibit a very similar response to the normalized peak stress data from Section 5.2 even though it was obtained from different tests. While the normalized peak stress was from a cyclic compression test, these are from a constant compression test. The elastic relaxation of the 500 nm LLZTO electrolytes provides

a more consistent mechanical behavior when compared to the no LLZTO electrolytes. This improvement in consistency translates to a better contact pressure between the electrolyte, cathode, and anode possibly leading to better charge capacity and charge cycle life in lithium-ion batteries.

5.4 Surface Roughness

Irregularities and inconsistencies in surface topography decrease the contact surface and directly affect the contact pressure of composite polymer electrolytes. The average surface roughness is used to quantify the topography of the CPEs. The surface roughness is found by finding the root mean square of a set of vertical position (z) values output by the optical profilometer as described in Section 4.4. Examples of the topographical plots created from those vertical position (z) values are shown in Figure 11.

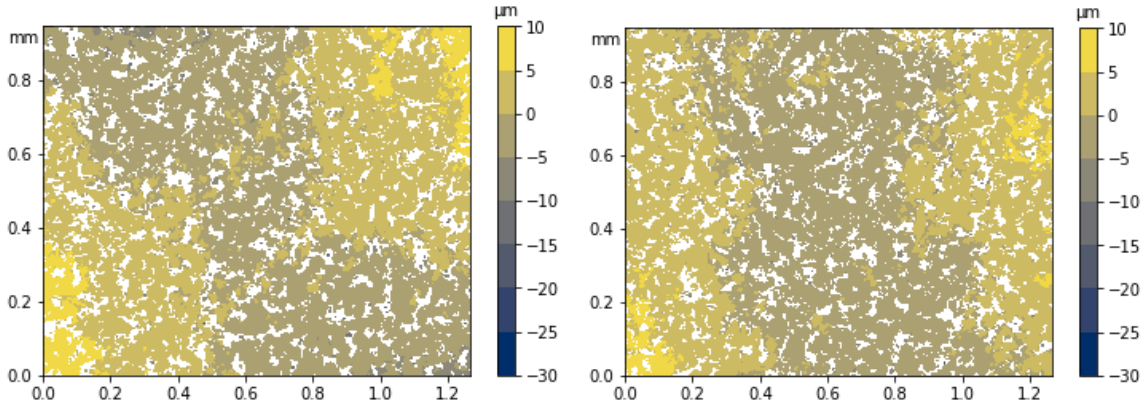

Figure 11. Optical profilometry plot showing the topography of the surface of a PEO specimen without any LLZTO as-fabricated (left) and cycled (right).

Quantitative differences are difficult to discern between the as-fabricated topographical plot on the left and the cycled plot on the right. However, the general trends of the peaks and

valleys of the surface topography can be seen in coupled images. The similarities in the topographical trends confirms that the fiducial marking process is successful in locating the same spot on the electrolyte specimen. In order to quantify the topography of the electrolytes that may not be discernible from the surface plots, Figure 12 compares the calculated surface roughnesses of the as-fabricated and cycled electrolytes. As seen in Figure 12, the surface roughness of the composite polymer electrolyte decreases by 16% on average from 2.59 µm as-fabricated to 2.17 µm after mechanical cycling. Undulations and irregularities are present in the as-fabricated specimens, and these surface roughness results prove that the cyclic compression process is helpful in removing some of these undulations and homogenizing the surface of the specimens.

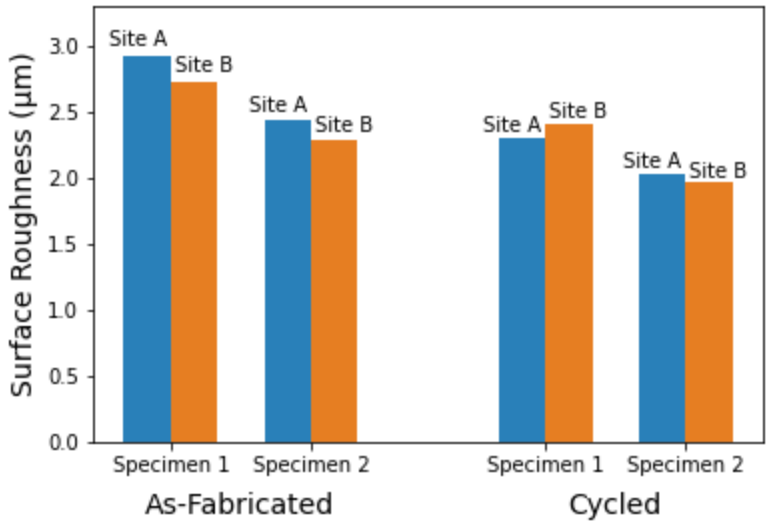

Figure 12. Comparison of the surface roughness of the CPE from before and after cycling, sampled at two sites each on two specimens.

Relating to the peak stress and stress relaxation plots, the undulations in the specimens cause the initial drop in stress that can be seen in Figures 7 and 10. While the homogenizing

effect of mechanical cycling could be a factor in the reduced fatigue softening that the 500 nm LLZTO specimens showed in Section 5.2, both the no LLZTO and the 500 nm LLZTO specimens would have experienced a similar effect of topographical homogenization, but the no LLZTO specimens continued to display clear fatigue softening over five hundred cycles that was counteracted by the 500 nm LLZTO electrolytes.

5.5 Thickness Measurements and Reproducibility

Another possible reason for the fatigue softening of the composite polymer electrolytes could have been a change in thickness affecting the contact pressure and internal stress of the CPEs. The specimen thickness was measured using a micrometer, before and after mechanical conditioning, denoted as "as-fabricated" and "cycled", respectively. The thickness measurements were measured with little compression on the specimens, close to the 70 mN preload detailed in Section 4.2. The specimens in this experiment used 600k g/mol PEO at a 43:1 EO:Li molar ratio and the specimens with 500 nm LLZTO particles had a 24 wt.% of LLZTO. Figure 13 shows a comparison of the specimen thicknesses for both types of specimens from before and after cycling. Based on the data from Figure 13, the variability of the specimen thickness did not change between as-fabricated and cycled. However, there was a slight increase in mean thickness from 55 μm to 57 μm for the no LLZTO electrolytes and from 42 μm to 44 μm for the 500 nm LLZTO electrolytes.

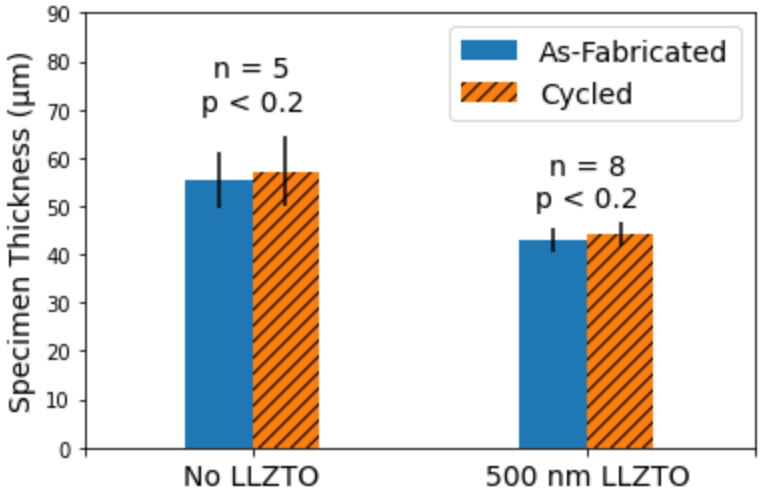

Figure 13. Comparison of the specimen thickness from before and after cycling for both No LLZTO electrolytes and 500 nm LLZTO electrolytes.

The increase in thickness was not statistically significant ($p > 0.1$, one-tailed). Therefore, it can be concluded that the change in thickness of the composite polymer electrolytes was not a contributing factor to fatigue softening in the electrolytes.

6. CONCLUSIONS

To restate and tie all of the experimental findings back into the hypothesis. The hypothesis of this investigation is that the addition of rigid particles to a composite polymer electrolyte counteracts the fatigue softening effect introduced by cyclic compression. The stress-strain curves show that CPEs with 500 nm LLZTO exhibit a 57% increase in peak stress at 30% strain compared to those without LLZTO. The difference in peak stresses establishes that even before investigating multiple cycles and viscoelastic responses, the 500 nm LLZTO CPE is stiffer than the no LLZTO CPE. The first time constant of the stress relaxation curve is 43% smaller for 500 nm LLZTO than for no LLZTO. The change in time constants means that 500 nm LLZTO has a faster, viscous response where the electrolytes relax quicker but to a smaller magnitude than their no LLZTO counterparts. Looking at the CPE response over 500 cycles, the no LLZTO electrolytes exhibit continual fatigue softening, with the average peak stresses declining by 25%. Comparatively, the 500 nm LLZTO seems to counteract the fatigue softening, with the average peak stresses only declining by 12%, almost half as much as the no LLZTO electrolytes. The compression process also decreases the surface roughness of the CPEs by 16%.

Relating the mechanical and viscoelastic results to battery technology, higher charging temperatures and thermal swelling cause electrolytes to experience up to 15% strain when approaching a fully charged state [2]. The stress-strain curve shows how an electrolyte will respond at higher strains and how much stress the electrolyte might experience. Each charge cycle for a battery can be up to three hours [5]. The viscoelastic response quantifies how an

electrolyte behaves throughout a single charge cycle, the elastic response of the 500 nm LLZTO electrolyte provides a more consistent mechanical behavior that in turn could stabilize battery performance. Battery cycle life can depend on the cathode and charging rates used, however, most lithium-ion batteries have a battery cycle life between 600 and 800 cycles [6]. Therefore, the normalized peak stress results offer an accelerated analog to the mechanical cycling of the electrolytes over the whole life of the battery. The 50% reduction in fatigue softening, when adding 500 nm LLZTO particles, is helpful to the long term stability and performance of the battery. Through both the stress relaxation and cyclic compression results, the 500 nm LLZTO electrolytes exhibit a more stable response, with less fatigue softening from both cyclic and constant compression. Fatigue softening in electrolytes can lead to weaker contact pressure between the cathode, anode, and electrolyte, resulting in a decrease in performance when compared to an ideal scenario without any changes in volume or pressure [7]. The increased stability of the 500 nm LLZTO composite polymer electrolytes helps to keep a more consistent contact pressure among battery components and is an improvement for battery performance.

A recommendation for future work that could build upon this thesis would be the thermomechanical effects of cyclic compression on composite polymer electrolytes. The thermomechanical study could investigate whether the increased stress from expansion would cause further increases in temperature in addition to the temperature increases that are already prevalent in the charging cycle. Another recommendation would be an investigation into the effects of cyclic compression on the particle distribution of LLZTO. The particle

distribution study could use imaging techniques to quantify whether the LLZTO particles form aggregates in the polymer after experiencing compression, which could cause localized stress concentrations in the areas of aggregation.

References Cited

[1] C. Wang, K. Fu, S. P. Kammampata, D. W. McOwen, A. J. Samson, L. Zhang, G. T. Hitz, A. M. Nolan, E. D. Wachsman, Y. Mo, V. Thangadurai, and L. Hu, "Garnet-Type Solid-State Electrolytes: Materials, Interfaces, and Batteries," *Chem. Rev.*, vol. 120, no. 10, pp. 4257–4300, May. 2020.

[2] K. Y. Oh, J. B. Siegel, L. Secondo, S. U. Kim, N. A. Samad, J. Qin, D. Anderson, K. Garikipati, A. Knobloch, B. I. Epureanu, C. W. Monroe, and A. Stefanopoulou, "Rate dependence of swelling in lithium-ion cells," *J. Power Sources*, vol. 267, pp. 197–202, Dec. 2014.

[3] T. Kelly, B. M. Ghadi, S. Berg, and H. Ardebili, "In Situ Study of Strain-Dependent Ion Conductivity of Stretchable Polyethylene Oxide Electrolyte," *Sci. Rep.*, vol. 6, p. 20128, Feb. 2016.

[4] W. S. Lee, K. S. Yeo, A. Andriyana, Y. G. Shee, and F. R. Mahamd Adikan, "Effect of cyclic compression and curing agent concentration on the stabilization of mechanical properties of PDMS elastomer," *Mater. Des.*, vol. 96, pp. 470–475, Apr. 2016.

[5] D. Zhang, B. S. Haran, A. Durairajan, R. E. White, Y. Podrazhansky, and B. N. Popov, "Studies on capacity fade of lithium-ion batteries," *J. Power Sources*, vol. 91, no. 2, pp. 122–129, Dec. 2000.

[6] Y. Yang, "A machine-learning prediction method of lithium-ion battery life based on charge process for different applications," *Appl. Energy*, vol. 292, p. 116897, Jun. 2021.

[7] E. Borgardt, L. Giesenberg, M. Reska, M. Muller, K. Wippermann, M. Langemann, W. Lehnert, and D. Stolten, "Impact of clamping pressure and stress relaxation on the performance of different polymer electrolyte membrane water electrolysis cell designs," *Int. J. Hydrogen Energy*, vol. 44, no. 42, pp. 23556–23567, Sep. 2019.

[8] R. Koerver, W. Zhang, L. de Biasi, S. Schweidler, A. Kondrakov, S. Kolling, T. Brezesinski, P. Hartmann, W. Zeier, and J. Janek, "Chemo-mechanical expansion of lithium electrode materials – on the route to mechanically optimized all-solid-state batteries," *Energy Environ. Sci.*, vol. 11, no. 8, pp. 2142–2158, Aug. 2018.

[9] J. H. Lee, H. M. Lee, and S. Ahn, "Battery dimensional changes occurring during charge/discharge cycles—thin rectangular lithium ion and polymer cells," *J. Power Sources*, vol. 119–121, pp. 833–837, Jun. 2003.

[10] J. Barker, “In-situ measurement of the thickness changes associated with cycling of prismatic lithium ion batteries based on LiMn2O4 and LiCoO2,” *Electrochim. Acta*, vol. 45, no. 1, pp. 235–242, Sep. 1999.

[11] D. Sauerteig, N. Hanselmann, A. Arzberger, H. Reinshagen, S. Ivanov, and A. Bund, “Electrochemical-mechanical coupled modeling and parameterization of swelling and ionic transport in lithium-ion batteries,” *J. Power Sources*, vol. 378, pp. 235–247, Feb. 2018.

[12] S. Patra, M. Yeddala, P. Daga, and T. N. Narayanan, “Anisotropic mechanical responses of poly(ethylene oxide)‐based lithium ions containing solid polymer electrolytes,” *Macromol. Chem. Phys.*, vol. 220, no. 21, p. 1900348, Nov. 2019.

[13] M. R. Mansouri, P. F. Fuchs, M. Baghani, and C. Schuecker, “Matrix–fiber interfacial debonding in soft composite materials: Cyclically behavior modeling and microstructural evolution,” *Composites Part B*, vol. 237, p. 109853, May. 2022.

[14] K. Y. Oh and B. I. Epureanu, “A novel thermal swelling model for a rechargeable lithium-ion battery cell,” *J. Power Sources*, vol. 303, pp. 86–96, Jan. 2016.

[15] M. V. F. Heinz, G. Graeber, D. Landmann, and C. Battaglia, “Pressure management and cell design in solid-electrolyte batteries, at the example of a sodium-nickel chloride battery,” *J. Power Sources*, vol. 465, p. 228268, Jul. 2020.

[16] E. M. C. Jones, M. N. Silberstein, S. R. White, and N. R. Sottos, “In Situ Measurements of Strains in Composite Battery Electrodes during Electrochemical Cycling,” *Exp. Mech.*, vol. 54, no. 6, pp. 971–985, Jul. 2014.

[17] H. Xie, Q. Zhang, H. Song, B. Shi, and Y. Kang, “Modeling and in situ characterization of lithiation-induced stress in electrodes during the coupled mechano-electro-chemical process,” *J. Power Sources*, vol. 342, pp. 896–903, Feb. 2017.

[18] G. J. Rees, D. Spencer Jolly, Z. Ning, T. J. Marrow, G. E. Pavlovskaya, and P. G. Bruce, “Imaging Sodium Dendrite Growth in All-Solid-State Sodium Batteries Using 23 Na T2 -Weighted Magnetic Resonance Imaging,” *Angew. Chem. Int. Ed Engl.*, vol. 60, no. 4, pp. 2110–2115, Jan. 2021.

[19] L. Albero Blanquer, F. Marchini, J. Seitz, N. Daher, F. Betermier, J. Huang, C. Gervillie, and J. M. Tarascon, “Optical sensors for operando stress monitoring in lithium-based batteries containing solid-state or liquid electrolytes,” *Nat. Commun.*, vol. 13, no. 1, p. 1153, Mar. 2022.

[20] S. Samal, “Effect of shape and size of filler particle on the aggregation and sedimentation behavior of the polymer composite,” *Powder Technol.*, vol. 366, pp. 43–51, Apr. 2020.

[21] K. Bouziane, E. M. Khetabi, R. Lachat, N. Zamel, Y. Meyer, and D. Candusso, “Impact of cyclic mechanical compression on the electrical contact resistance between the gas diffusion layer and the bipolar plate of a polymer electrolyte membrane fuel cell,” *Renewable Energy*, vol. 153, pp. 349–361, Jun. 2020.

[22] T. J. Mason, J. Millichamp, P. R. Shearing, and D. J. L. Brett, “A study of the effect of compression on the performance of polymer electrolyte fuel cells using electrochemical impedance spectroscopy and dimensional change analysis,” *Int. J. Hydrogen Energy*, vol. 38, no. 18, pp. 7414–7422, Jun. 2013.

[23] J. F. Vélez, M. Aparicio, and J. Mosa, “Covalent silica-PEO-LiTFSI hybrid solid electrolytes via sol-gel for Li-ion battery applications,” *Electrochim. Acta*, vol. 213, pp. 831–841, Sep. 2016.

[24] J. Li, J. Zhang, H. Zhai, X. Tang, and G. Tan, “Rapid synthesis of garnet-type Li7La3Zr2O12 solid electrolyte with superior electrochemical performance,” *J. Eur. Ceram. Soc.*, vol. 42, no. 4, pp. 1568–1575, Apr. 2022.

[25] J. Yin, X. Xu, S. Jiang, H. Wu, L. Wei, Y. Li, J. He, K. Xi, and Y. Gao, “High ionic conductivity PEO-based electrolyte with 3D framework for Dendrite-free solid-state lithium metal batteries at ambient temperature,” *Chem. Eng. J.*, vol. 431, no. 3, p. 133352, Mar. 2022.

[26] A. Gupta and J. Sakamoto, “Controlling Ionic Transport through the PEO-LiTFSI/LLZTO Interface,” *Electrochem. Soc. Interface*, vol. 28, p. 63, Jul. 2019.

[27] I. Halabi, “Viscoelasticity in Particle-Loaded PEO Gels Under Compression for Mimicking Mechanical Changes in Lithium-Ion Batteries,” M.S. thesis, Mech. Engr., SJSU, San Jose, CA, Nov. 2020.

[28] N. Mulay, D. Oh, D.-I. Yoon, and S.-J. (John) Lee, “Effect of Cyclic Compression on Mechanical Behavior of Ceramic-in-Polymer Composite Electrolytes for Lithium-Ion Batteries,” presented at IMECE, USA, November 1-5, 2021, Paper 69196.

[29] C. G. Abraham, “Ionic Percolation Networks in Composite Electrodes for All-Solid-State Batteries,” M.S. thesis, Chem. and Mat. Engr., SJSU, San Jose, CA, Nov. 2021.

[30] M. A. Del Nobile, S. Chillo, A. Mentana, and A. Baiano, “Use of the generalized Maxwell model for describing the stress relaxation behavior of solid-like foods,” *J. Food Eng.*, vol. 78, no. 3, pp. 978–983, Feb. 2007.

[31] F. Renaud, J.-L. Dion, G. Chevallier, I. Tawfiq, and R. Lemaire, “A new identification method of viscoelastic behavior: Application to the generalized Maxwell model,” *Mech. Syst. Signal Process.*, vol. 25, no. 3, pp. 991–1010, Apr. 2011.

[32] J. A. Epaarachchi, “17 - The effect of viscoelasticity on fatigue behaviour of polymer matrix composites,” in *Creep and Fatigue in Polymer Matrix Composites*, R. M. Guedes, Ed., Sawston, U.K.: Woodhead Publishing, 2011, pp. 492–513.

[33] M. A. Del Nobile, S. Chillo, A. Mentana, and A. Baiano, “Use of the generalized Maxwell model for describing the stress relaxation behavior of solid-like foods,” *J. Food Eng.*, vol. 78, no. 3, pp. 978–983, Feb. 2007.

[34] R. G. Airapetyan and A. G. Ramm, “Numerical Inversion of the Laplace Transform from the Real Axis,” *J. Math. Anal. Appl.*, vol. 248, no. 2, pp. 572–587, Aug. 2000.

[35] A. Caponnetto and E. De Vito, “Optimal Rates for the Regularized Least-Squares Algorithm,” *Found. Comut. Math.*, vol. 7, no. 3, pp. 331–368, Jul. 2007.

[36] Q. Liu, Z. Geng, C. Han, Y. Fu, S. Li, Y. B. He, F. Kang, and B. Li, “Challenges and perspectives of garnet solid electrolytes for all solid-state lithium batteries,” *J. Power Sources*, vol. 389, pp. 120–134, Jun. 2018.

[37] J. R. Cotton, K. Winwood, P. Zioupos, and M. Taylor, “Damage rate is a predictor of fatigue life and creep strain rate in tensile fatigue of human cortical bone samples,” *J. Biomech. Eng.*, vol. 127, no. 2, pp. 213–219, Apr. 2005.

[38] S. M. Asadul Hossain and M. Saitou, “Surface roughness of thin silver films pulse-plated using silver cyanide-thiocyanate electrolyte,” *J. Appl. Electrochem.*, vol. 38, no. 12, pp. 1653–1657, Dec. 2008.

[39] D. Montgomery and G. Runger, *Applied Statistics and Probability for Engineers*, 6th ed. Hoboken, New Jersey, U.S.A: John Wiley & Sons, 2013.